Verification of Tire Hydroplaning Phenomenon Using Coupled FSI Simulation by CFD and FEM

Hyun Chul Jung[1], Mi Dum Jung[2], Kyoung Moon Jeong[1*], Kyunghoon Lee[2]

[1]Design Automation & Simulation Team, R & D Center, KUMHO TIRE Co. Inc., Yongin-si, Gyeonggi-do, South Korea
[2]Solution Lab Co., 20 Dunsanjung-ro, Seo-gu, Daejeon, South Korea
Email: jhc111@kumhotire.com, mujung@solution-lab.co.kr, *kmjeong@kumhotire.com, klee@solution-lab.co.kr

Abstract

Hydroplaning phenomenon is one of the major factors that must be considered to ensure safe driving on wet road surfaces. In this paper, the approach to numerical simulation of the physical hydroplaning characteristics using patterned tire is described. A detailed 3-D patterned tire model is constructed by in-house modeling program and the water flow is considered as incompressible. The complex tire material compositions are effectively modeled using composites, and rubber properties generalize the Mooney-Rivlin model. The finite element method (FEM) and the advanced finite volume method (FVM) are used for structural and for fluid-tire interaction analysis, respectively. Performance prediction of hydroplaning via coupling of computational fluid dynamics (CFD) and FEM has delivered a detailed insight into the local mechanisms and root causes of hydroplaning. Numerical examples were verified by comparing the experimental test results and it is confirmed to indicate similar correlation tendency and high reliability. The effect of driving velocity, pattern groove size, and pattern direction on hydroplaning phenomenon of tire is discussed and logical results were obtained.

Keywords

Tire, Hydroplaning, Finite Element Method, Computational Fluid Dynamic, Fluid Structure Interaction

1. Introduction

Tire is the only part of the vehicle that contacts with the road surface and force-transmitting of steering. When a vehicle is driving on wet road surface at high speed, the water flow through the tire tread grooves generates the hydrodynamic pressure and loses the contact pressure. The occurrence of this hydro-

dynamic lift force deteriorates not only the tire traction efficiency but also the driving and the braking performance become worse [1] [2] [3] [4]. In particular, tire driving performances on wet road surface are considerably important to tire manufacturing companies because the labeling regulation classifies wet grip as a major issue. The effects of many factors on hydroplaning were investigated in experimental works, such as road texture, inflation pressure, tire velocity, tread pattern, load, water depth and so on [5] [6] [7] [8]. Studies of tire performance on wet road surface have been actively conducted until now, but are still time-consuming and extensive. So many engineers and researchers have studied the hydroplaning phenomena. Aksenov *et al.* [9] built a three-dimensional simulation model of the interaction between tire and water flow using CFD method. Tire surface deformation was ignored in their model; however, the computational domain remained fixed in time. The influence of hydrodynamic pressure on smooth and grooved tires with deformation was considered and the results were compared with that of the un-deformed tires. The results showed that tire deformation has a big effect on hydrodynamic pressure at higher tire speed. Seta *et al.* [10] adopted the finite difference method (FDM) and FEM to simulate hydroplaning on thick water-films, under different parameters such as water-flow, speed dependence, and tread pattern effects. Although the viscosity of water was ignored in this simulation, these parameters could be predicted qualitatively. They found that a sloped block tip can effectively improve tire hydroplaning performance. Okano and Koich [11] were used to solve the coupled problems between tire deformation and fluid flow. Tire deformation is solved using FEM and fluid behavior is solved using FVM. Cho *et al.* [12] compared hydroplaning speed between different patterned tires, and they found that hydroplaning performance largely depends on the structure parameters of the tread pattern. A stable and reliable numerical procedure to simulate and investigate the tire hydroplaning phenomenon has been presented by generally coupling the finite volume method and the explicit FEM. Fwa *et al.* [13] established a numerical simulation model using CFD techniques implemented in Fluent to study the effects of vertical and horizontal circumferential groove dimension on hydroplaning. They found that larger groove width and depth and smaller groove spacing can help improve hydroplaning performance. Guo *et al.* [14] implemented CFD and FEM techniques to solve the hydroplaning effect. The results show that when the standing water depth is far less than the tire tread groove depth (5 - 8 mm), the tire tread grooves can completely drain water. But standing water depth closes to (or large than) tire tread depth, the tire tread grooves cannot drain off hydrops in the tire grooves completely and the action coverage of the high pressure induced by hydrodynamic pressure will occur in the front of the tire. It was suggested that a car should travel at mid or low speed (65 to 85 km/h) on wet roads.

Rotated tire numerical simulation on fluid flow is one of the challenging problems for CFD. In most CFD solver, the tire model is considered a rigid body

without rotation or deformation. The adequate numerical method which allow to overcome these difficulties is needed to solve the problems. The main object of this paper is to study utilization of Flowvision-Abaqus co-simulation [15] [16] method to analyze tire hydroplaning effects on wet roads. Use of these co-simulation allows to analyze an interaction between tire deformation/rotation and complex gas/fluid flows. To verify the effectiveness of the method, predicted hydroplaning performance of four different simplified tread patterns is compared with experiments.

2. Method of Simulation

2.1. Tire FE Modeling

Different components of a typical radial tire are shown in **Figure 1**. Each component has been designed to comply with the rubber and cord composite in addition to several specific factors for driving performance. These take an important role in maintaining the stiffness and strength required in a tire. The roles of each part are well described in a book by Lindenmuth [17]. The components are composed of several rubber components and fiber-reinforced components such as radial carcass plies, belt plies, bead wires, and so on. A great portion of the tire structure consists of vulcanized rubber. The rubber has a nonlinear and incompressible behavior towards loading which is independent of the strain rate. The nonlinear elastic material response is formulated by a strain energy density function accounting for large strain components. The strain energy density function is defined according to the penalized first-order Mooney-Rivlin model in which the strain density function is defined by

$$W\left(J_1, J_2, J_3 : K\right) = C_{10}\left(J_1 - 3\right) + C_{01}\left(J_2 - 3\right) + \frac{K}{2}\left(J_3 - 3\right)^2 \tag{1}$$

where J_i is the invariants of the Green-Lagrangian strain tensor and C_{10} and C_{01} are the rubber material constants determined from the experiment. On the other hand, K is a sort of penalty parameter controlling the rubber incompressibility. The shear modulus τ and the bulk modulus κ of rubber are related as $2\left(C_{10} + C_{01}\right) = \tau$ and $K = 2\kappa$, from which one can easily obtain the following relation for Poisson's relation:
$v = \left[3K/4\left(C_{10} + C_{01}\right) - 2\right] / \left[3K/2\left(C_{10} + C_{01}\right) + 2\right]$ [16]. It is clear that the incompressibility of rubber is asymptotically enforced as the penalty parameter approaches infinity, but the choice of K near 100 is usually recommended for the stable transient dynamic response with the reasonable time step size. The fiber reinforced components are the predominant load carrying members of the cord-rubber composite. They provide strength and stability to the sidewall and tread as well as contain the air pressure. Since the fiber reinforced components parts are in the highly complex structure, the material models are chosen by the objective of the numerical simulation. In the tire analysis, the fiber reinforcement components in the model were modeled using special purpose rebar shell
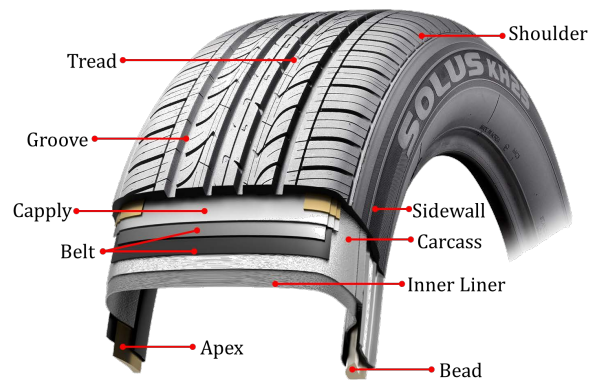
Figure 1. Tire structure and components.

elements. The rebar layers were embedded in the 3D solid by defining the nodes for rebar element. The embedded rebar elements were constrained to move relative host elements by a kinematic coupling which enforces the position of the host nodes and embedded rebar elements nodes to have a mutually linear dependency. In this study, two belt layers and carcass with embedded rebar elements are modeled. Meanwhile, steel cord and rubber matrix of the bead area is modeled as a homogeneous solid. **Figure 2** shows a two-dimensional section mesh constructed according to the above-mentioned material modeling such that pure rubber solid, composite shell and homogenized solid elements are mixed.

2.2. Model Setup of FSI Simulation

The CFD package from Capvidia [15] was developed as wide application tool for study of complex gas/fluid flows. And FE software from SIMULIA [16] provides many functions of tire simulation such as embedded element technique for composite and enables steady state simulations in order to reduce the analysis time and so on. To solve hydroplaning simulation, CFD code Flowvision and FE code ABAQUS which are strongly coupled for bidirectional fluid structure interaction (FSI) co-simulation are implemented. An axisymmetric structural part and a non-symmetrical tread part are consisted in the tire model. Tread geometry is obtained by assembling a sequence of pitches. A vertical load is then applied, and using steady state transport analysis, the tire will reach a stationary rolling condition at travelling speed. When the tire FE model is completed, tread surface geometry of tire FE model is imported into CFD code as shown in **Figure 3**. CFD code uses the interactive interface to create computational fluid domain for hydroplaning simulation, and specify appropriate boundary conditions such as flow velocity and flow inlet/outlet etc.

After then Abaqus/explicit analysis will start to co-simulate with CFD software, to simulate the tire rolling over water films and investigate the performance of tire wet-grip capabilities. The whole analysis procedure is shown in **Figure 4**.
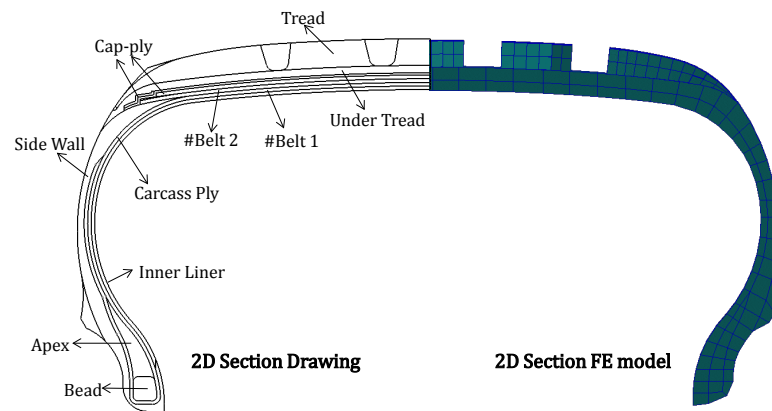
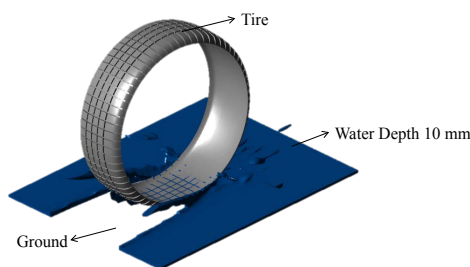**Figure 2.** The 2D section drawing and finite element model of the tire.

Figure 3. Computational structure and fluid domain.
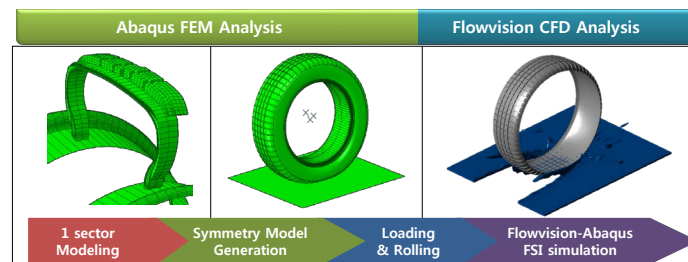

Figure 4. Analysis procedure of FSI co-simulation for tire hydroplaning.

2.3. Sub-Grid Geometry Resolution Method

The link between FE and CFD meshes is built automatically via Flowvision Sub-Grid Geometry Resolution (SGGR) technique [18] [19]. The SGGR technology allows to import the CAD file to the computational domain without any feature loss, thus both saving man hour for meshing and letting the engineering focus on the physics of the problem to be solved. Theoretically, common CAD systems can generate the description of object surface by a set of plane facets. Using this representation allows for CFD code to perceive geometry information from CAD through FEM coupling. In this case, the CFD code becomes compatible with other CAE systems based on finite element analysis. Let the adaptive locally refined grid (ALGR) has given in computational domain. At first stage of algorithm the facets intersecting the grid cell are being found. Then the grid cell is disjoined into a set of finite volumes bounded by facets and cell faces. If the

cell does not intersect any facet, the finite volume coincides with cell as shown in **Figure 5**. With the help of this technology, it can make program deal with the tire with complex tread pattern rolling in computational domain without problem of distortion of computational grid.

2.4. Governing Equations

In this paper, water flow assumes that it is governed by system of equations for incompressible fluid which includes continuity and Navier-Stokes equations [19]. To consider the algorithm of the equations solving again write ones in Lagrange integral form for volume moved with fluid during intermitted time duration is:

$$\frac{\partial_p}{\partial_t} + \nabla \cdot (\rho V) = 0 \tag{2}$$

$$\frac{\partial_p V}{\partial_t} + \nabla \cdot (\rho V \otimes V) = -\nabla P + \nabla \cdot \hat{\tau}_{eff} + \rho F \tag{3}$$

Equations (2) and (3) were used to solve the velocity and pressure of fluid with a decouple process called as pressure and velocity split process [9]. Here, $\hat{\tau}_{eff}$ is the effective shear stress tensor caused by viscosity of fluid. The turbulence of water flow around the rolling tire is also considered. The standard K-ε model, expressed as (4) and (5) is used to solve the turbulent energy and dissipation of fluid.

$$\frac{\partial (pk)}{\partial t} + \nabla \cdot (\rho V k) = \nabla \left(\left(\mu + \frac{\mu_t}{\sigma_k} \right) \nabla k \right) + \mu_t \left(G + \frac{\beta}{Pr_t} g \cdot \nabla T \right) - \rho \varepsilon \tag{4}$$

$$\frac{\partial (p\varepsilon)}{\partial t} + \nabla \cdot (\rho V \varepsilon) = \nabla \left(\left(\mu + \frac{\mu_t}{\sigma_k} \right) \nabla \varepsilon \right) + C_1 \frac{\varepsilon}{k} \mu_t \left(G + \frac{\beta}{Pr_t} g \cdot \nabla T \right) - C_2 \rho \frac{\varepsilon^2}{k} \tag{5}$$

The model parameters and the expression for generating term G can be rewritten as (6), (7), and (8):

$$G = D_{ij} \frac{\partial V_i}{\partial_{xj}} \tag{6}$$

$$D_{ij} = S_{ij} - \frac{2}{3} \left(\nabla \cdot V + \frac{\rho k}{\mu_t} \right) \delta_{ij} \tag{7}$$

$$S_{ij} = \frac{\partial V_i}{\partial x_j} + \frac{\partial V_j}{\partial x_i} \tag{8}$$

The object of this study is to investigate the resistance force of a rolling tires caused by fluid-dynamic, we will be introduced the similarity approach to experimentally measure the resistance of a tire rolling in a basin instead of wind tunnel for the validation of simulation. Therefore, the working fluid in this simulation is water, and heat transfer can be neglected reasonably. The units and numerical settings are listed in **Table 1**. Equation (9) was used to solve the total pressure of fluid, and the total resistance force of a rolling tire is calculated by Equation (10)
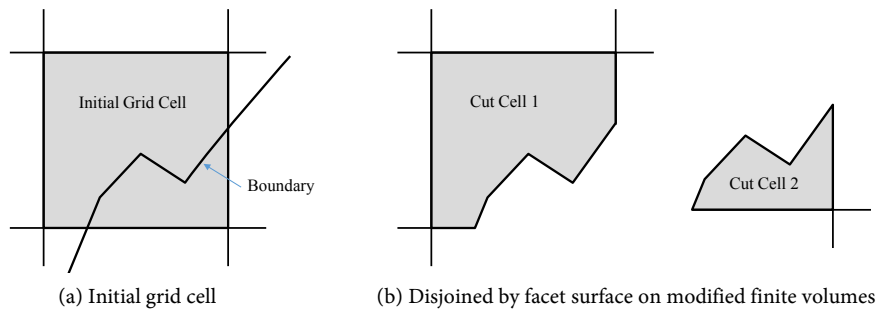
Figure 5. Sub-grid geometry resolution [18].

$$P_{tot} = P + P_{hst} + \frac{1}{2}\rho|V_{abs}|^2 \tag{9}$$

$$F_{\text{fluid}} = \oint_s (P + P_{hst}) n\,dS - \oint_s (\mu + \mu_t)\frac{\partial V}{\partial n}\,dS \tag{10}$$

The free surface flow is modeled by the "Advanced VOF model" in Flowvision [15]. Transfer of the water phase boundary is described by the equation for the volume fraction of this (continuous) phase in a computational cell ("Volume Of Fluid" = VOF). Variable VOF takes values from 0 (Gas) to 1 (Liquid). A cell, where 0 < VOF < 1, contains a contact surface. In the solver, this surface is represented by a set of polygons. Propagation of the volume fraction of water is solved by the transport Equation (11).

$$\frac{\partial F}{\partial T} + V \cdot \nabla F = 0 \tag{11}$$

3. Hydroplaning Analysis

3.1. Numerical Experiments of Hydroplaning

A representative tire model of passenger car is implemented to evaluate performance of hydroplaning. The size of tire is 205/55 R16 with simple tread pattern. Figure 6 and Figure 7 show the results of hydroplaning simulation. In Figure 6, velocity contour describes how the water flows through the channels of the treads. Also contact pressure plot indicates significant loss of contact force which is consistent with the buoyancy force as shown in Figure 7. The reason why the buoyancy increases rapidly and stabilizes at the start of the analysis is due to the initial speed and damping of the fluid and tire, and does not have any special meaning. As described above, the simulation results of hydroplaning were analyzed through buoyancy of FVM and contact force of FEM. Buoyancy is value caused by water pressure, large value means that hydroplaning performance is not good. But, contact force means force between tire and road, high value means good performance. The oscillations in the buoyancy force as shown in Figure 7 are due to the tread pattern surface and water flow. Despite the co-simulation of two different softwares, the tendency of buoyancy and contact pressure seems to be very well.

Table 1. Equation notation.

Notation	Physical quantity	Notation	Physical quantity
C_P	Specific heat	P_{tot}	Total pressure
G	Gravity acceleration	Pr_t	Turbulent prandtl number
H	Total enthalpy	T_{tot}	Total temperature
K	Turbulent energy	T_{ref}	Reference temperature
L	Characteristic length	T_{abs}	Absolute temperature
M	Molar mass	μ	Molecular dynamic viscosity
P	Relative pressure	μ_t	Turbulent dynamic viscosity
P_{ref}	Reference pressure	V	Relative velocity
P_{hst}	Hydrostatic pressure	ε	Dissipation rate of turbulent energy
P_{abs}	Absolute pressure	β	coefficient of thermal expansion
F	Variable of VOF	∂T	relative local specific

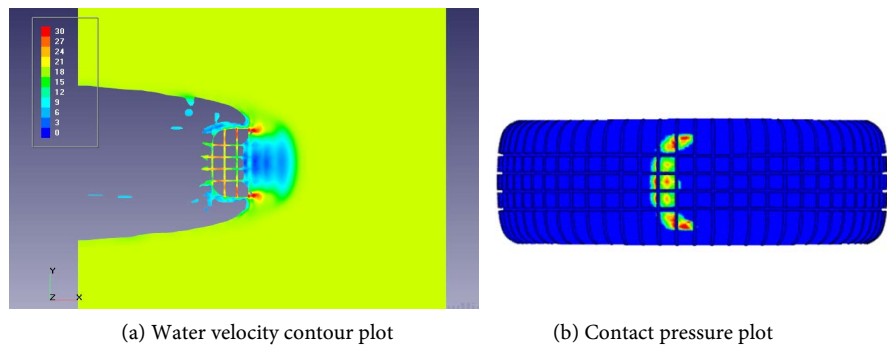(a) Water velocity contour plot (b) Contact pressure plot

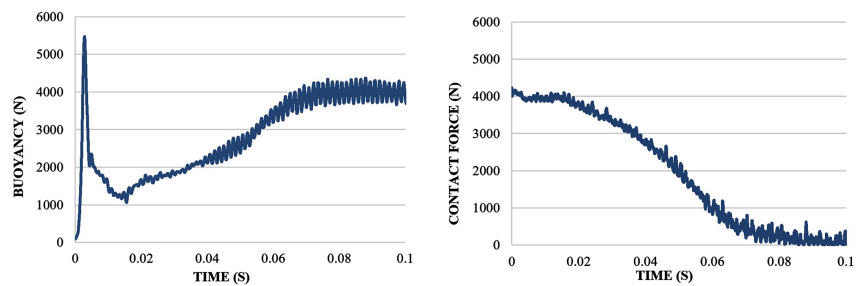**Figure 6.** Hydroplaning simulation results.

Figure 7. Buoyancy force and contact force between tire and road.

3.2. Verification of Hydroplaning

Four different test tires with simplified tread patterns were produced and experiments evaluating of longitudinal hydroplaning test were carried out. **Figure 8** shows the tire shape which actually manufactured and was designed considering the pattern design factor. In order to confirm a difference in the results of hydroplaning analysis of the tire, each version of tire is considered to give 3% - 7% design changes such as longitudinal/lateral groove, location/orientation of void

and angle of tread block. **Figure 9** shows a test of hydroplaning at the proving ground. Longitudinal hydroplaning test is for evaluating tire's hydroplaning performance during straight line driving on wet surface.

The measurement of hydroplaning performance by test tire is carried out on hydroplaning trailer. The hydroplaning trailer should be connected to a tow vehicle and drive left side of trailer to the wet test road. Then, measures speed of the test tire of left side of trailer and the tow vehicle. After that, calculate the hydroplaning occurred speed by compare speed of between the test tire and the vehicle. Specific test conditions are listed in **Table 2**. In the experiment, the relationships between vehicle velocity and slip ratio of each tire were measured for a vehicle running on a pool of water whose water depth is 10 mm. Tire slip ratio in the experiment is defined as follows.

$$\text{Slip ratio} = 1 - \frac{\text{Velocity of a tire}}{\text{Velocity of a trailor}} \quad (12)$$

The experimental rating indicates the trailer velocity, when the slip ratio is 10%. This is the way to obtain result in general experimental methods. The computational results used the contact force, when the simulation result is in stable.

| (a) PTN01 | (b) PTN02 | (c) PTN03 | (d) PTN04 |

Figure 8. Tires for hydroplaning test.

Figure 9. Hydroplaning test in proving ground.

Table 2. Test condition for hydroplaning.

Tire Type	Passenger Car Tire
Tire Size	205/55 R16
Rim	16 × 6.5 J
Inflation Pressure	207 kPa
Water Depth	10 mm

Figure 10 shows the buoyancy result images between tires during rotates at high speed and water. Since PTN01 is receiving more buoyancy than PTN04, it can be expected that the performance will be inferior from the pressure distribution range. The buoyancy of PTN02 and PTN03 is shown similar performance in hydroplaning simulation. The result comparison between the contact force of simulation and the experimental test is shown in **Figure 11**. The hydroplaning simulation using 3D patterned tires has similar results with the proving ground test. The tendency of proving ground test can be interpreted in the same with hydroplaning simulation, PTN04 > PTN03 > PTN02 > PTN01. Little difference of the value among each version is likely to be a common error in proving ground testing, so the results of the hydroplaning simulation have a high reliability with experimental test.

4. Parametric Study

Several different conditions were analyzed to confirm the consistency of the analysis procedure and results. Basically, the analysis results according to the driving velocity (50, 60, 70, 80, 90 km/h) were compared. And also the results according to the pattern shape were compared, because the pattern design factor had a dominant influence on the hydroplaning phenomenon.

4.1. Effect of Velocity

To find out how the hydroplaning characteristics change at different speed, the same passenger car tire model is used to carry out the simulations at different speeds. **Figure 12** shows contact pressure results at different vehicle speeds 50 km/h - 90 km/h, and **Figure 13** shows the buoyancy and contact pressure plots. Hydroplaning performance based on speed was verified to produce reasonable results. At lower speeds, the hydroplaning performance was better, but hydroplaning at higher speeds was worse in buoyancy and contact force. The results indicate that as speed increased, the tire completely loses contact force with the road surface at 90 km/h. This result is meaningful in various aspects, and it can be considered to be similar to the results of Guo *et al.* [14] that it is necessary to drive below 90 km/h on wet surface road in a rainy day.

4.2. Effect of Pattern Groove Width

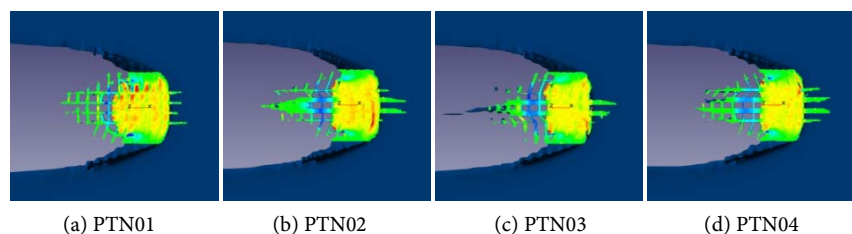In a tire pattern design, the width of the longitudinal groove is one of the most

| (a) PTN01 | (b) PTN02 | (c) PTN03 | (d) PTN04 |

Figure 10. Buoyancy pressure plot in hydroplaning simulation.
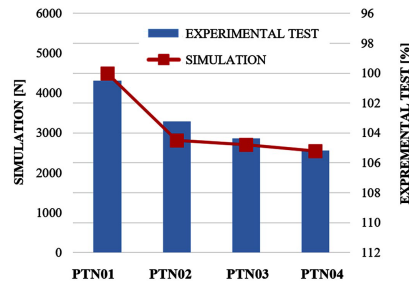
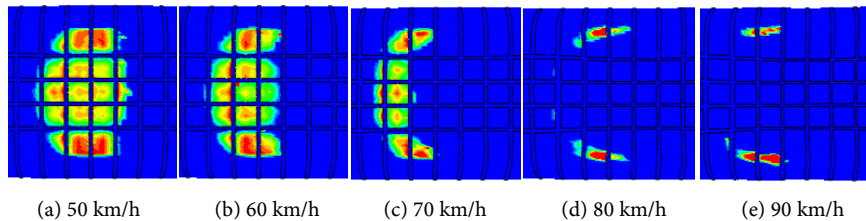**Figure 11.** Comparison between experiment and simulation.

| (a) 50 km/h | (b) 60 km/h | (c) 70 km/h | (d) 80 km/h | (e) 90 km/h |

Figure 12. Contact pressure plots at different velocities.

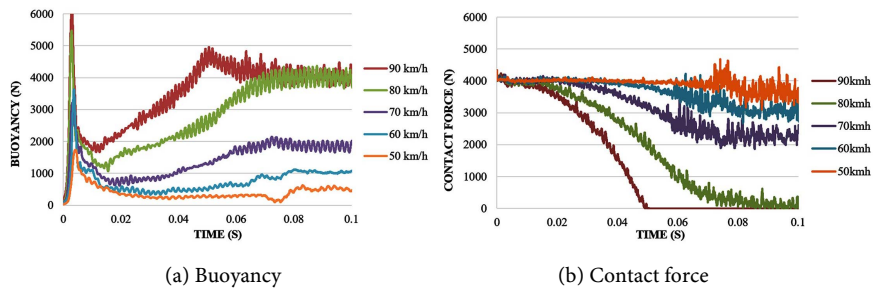| (a) Buoyancy | (b) Contact force |

Figure 13. Buoyancy force and reaction force between tire and road.

important factors to tire. It is necessary to increase the width of the groove to improve wet performance. In this section, hydroplaning simulation according to change groove width was conducted as shown in **Figure 14**. From Ver1 to Ver3, the width of tread groove is increased by 1 mm. **Figure 15** and **Figure 16** show the contact pressure results, buoyancy and road reaction force. In the contact pressure, there were no significant changes in water pressure. However, in buoyancy and contact force, we identified logical results that improved performance as the width of the grooves increased.

4.3. Effect of Pattern Direction

Since the V-shape grooved tire has different hydroplaning velocities according to the normal and reverse rotational directions a closer look will be taken at this tread pattern design as shown in **Figure 17**. Generally, these tires show better performance in forward rotation than reverse direction. As shown in **Figure 18**, the tire rotating in reverse direction quickly loses contact force between tire and road. And, tire that rotates in reverse direction showed an early increase in buoyancy. Vorticity, which indicates turbulence, is recommended to develop from the groove of tread to the outside because it affects water drainage. The vor-

ticity of the forward direction tire occurs much more in the tire rotation direction, while the reverse tire can be seen to occur a lot in front of rolling direction as shown in **Figure 19**. It can be expected that the interference of the fluid flow will eventually lead to an increase in pressure and eventually the performance of the tire will deteriorate.
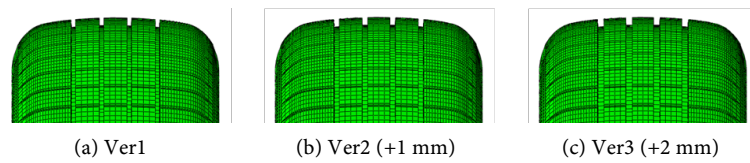

(a) Ver1   (b) Ver2 (+1 mm)   (c) Ver3 (+2 mm)

Figure 14. Tire modeling with variation of groove width.

(a) Ver1   (b) Ver2   (c) Ver3
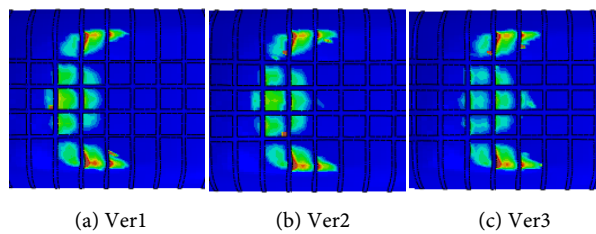
Figure 15. Contact pressure with variation of groove width.

(a) Buoyancy   (b) Contact force
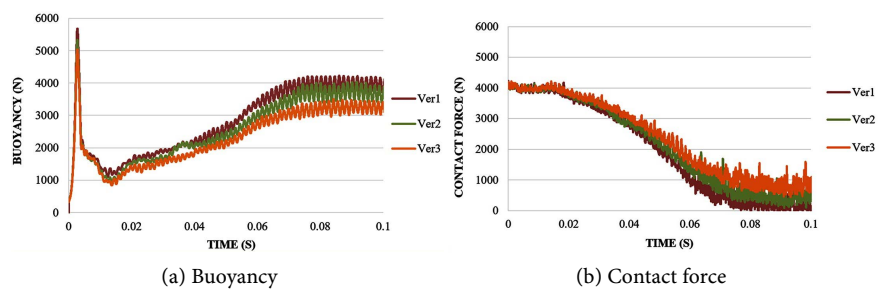
Figure 16. Buoyancy force and reaction force between tire and road.

Normal driving direction   Reverse driving direction
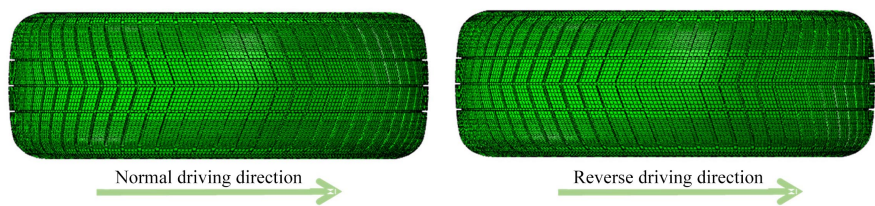
Figure 17. Tire modeling with V-shape grooved pattern.

(a) Buoyancy   (b) Contact force
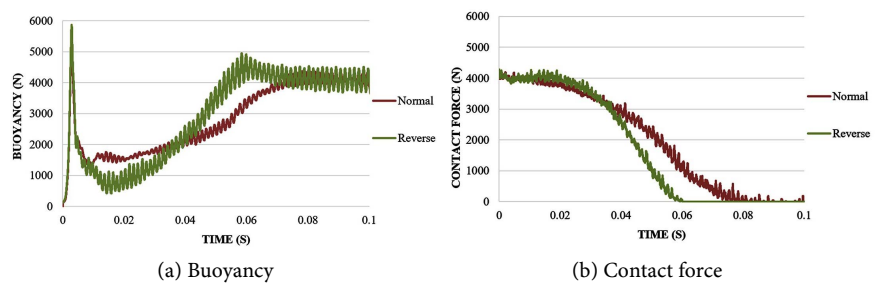
Figure 18. Buoyancy force and reaction force in V-shape pattern.
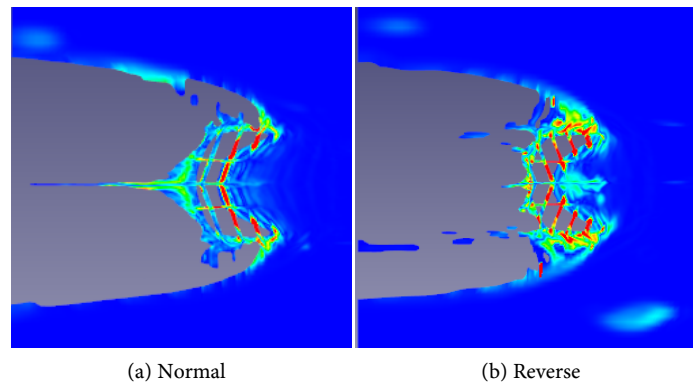
(a) Normal   (b) Reverse

Figure 19. Vorticity (turbulence) plot in V-shape pattern.

5. Conclusion

A numerical method for predicting hydroplaning performance has been introduced in this paper using the coupling of CFD and FEM. The tire rotation which is difficult to apply in the general CFD solver was reflected, and the SGGR technique enables to detail fluid flow with complex tread pattern rolling in the computational domain without any feature loss. As compared hydroplaning performance, the simulation results were analyzed through buoyancy and contact force. Buoyancy is value caused by water pressure, large value means that hydroplaning performance is not good. But, contact force means force between tire and road, high value means good performance. To verify the effectiveness of the method, hydroplaning performance of four different simplified tread patterns are compared with experiments. It is confirmed that results agree well with each other for the cases considered. Furthermore, predicted water flows around the contact patch area agree well with those experimental phenomena. These agreements are thought to support the effectiveness of the present hydroplaning simulations. The effect velocity, groove size and directional patterns on the tire hydroplaning phenomenon were analyzed to confirm the consistency of the analysis procedure and results and logical results were obtained. As a result, the new numerical procedure proposed here enables one to predict the process of the hydroplaning of a tire and the difference of the hydroplaning performance dependent on the effect of the tread pattern and its geometry quantitatively. To obtain a more accurate analysis, it is required to proceed with the study applying the precise friction coefficient due to contact between tread rubber and the wet road in the future. It is expected that these frictional characteristics can be extended to simulate braking and handling performance on wet road.

Acknowledgements

Conflicts of Interest

The authors declare no conflicts of interest regarding the publication of this paper.

References

[1] Wies, B., Roeger, B. and Mundl, R. (2009) Influence of Pattern Void on Hydroplaning and Related Target Conflicts. *Tire Science and Technology*, **37**, 187-206. https://doi.org/10.2346/1.3137087

[2] Browne, A.L. (1975) Tire Deformation during Dynamic Hydroplaning. *Tire Science and Technology*, **3**, 16-28. https://doi.org/10.2346/1.2167192

[3] Agrawal, S.K. and Henry, J.J. (1980) A Simple Tire Deformation Model for the Transient Aspect of Hydroplaning. *Tire Science and Technology*, **8**, 23-36. https://doi.org/10.2346/1.2151019

[4] Lee, K.S. (1998) Effects of Sipes on the Viscous Hydroplaning of Pneumatic Tires. *Tire Science and Technology*, **26**, 23-35. https://doi.org/10.2346/1.2135955

[5] Matilainen, M. and Tuononen, A. (2015) Tyre Contact Length on Dry and Wet Road Surfaces Measured by Three-Axial Accelerometer. *Mechanical Systems and Signal Processing*, **52-53**, 548-558. https://doi.org/10.1016/j.ymssp.2014.08.002

[6] Kim, S., Jeong, W., Park, Y. and Lee, S. (2006) Prediction Method for Tire Air-Pumping Noise Using a Hybrid Technique. *Journal of the Acoustical Society of America*, **119**, 3799-3812. https://doi.org/10.1121/1.2200140

[7] Grogger, H. and Weiss, M. (1996) Calculation of the Three-Dimensional Free Surface Flow around an Automobile Tire. *Tire Science and Technology*, **24**, 39-49. https://doi.org/10.2346/1.2137511

[8] Grogger, H. and Weiss, M. (1997) Calculation of Hydroplaning of a Deformable Smooth-Shaped and Longitudinally-Grooved Tire. *Tire Science and Technology*, **25**, 265-287. https://doi.org/10.2346/1.2137544

[9] Aksenov, A.A., Dyadkin, A.A. and Gudzovsky, A.V. (1996) Numerical Simulation of Car Tire Aquaplaning. In: *Computational Fluid Dynamics*, John Wiley & Sons, Hoboken, 815-820.

[10] Nakajima, Y. and Seta, E. (2000) Hydroplaning Analysis by FEM and FVM: Effect of Tire Rolling and Tire Pattern on Hydroplaning. *Tire Science and Technology*, **28**, 140-156. https://doi.org/10.2346/1.2135997

[11] Okano, T. and Koishi, M. (2001) A New Computational Procedure to Predict Transient Hydroplaning Performance of a Tire. *Tire Science and Technology*, **29**, 2-22. https://doi.org/10.2346/1.2135228

[12] Cho, J.R., Lee, H.W. and Sohn, J.S. (2006) Numerical Investigation of Hydroplaning Characteristics of Three-Dimensional Patterned Tire. *European Journal of Mechanics*, **25**, 914-926. https://doi.org/10.1016/j.euromechsol.2006.02.007

[13] Fwa, T.F., Pasindu, H.R. and Ong, G.P. (2011) Critical Rut Depth for Pavement Maintenance Based on Vehicle Skidding and Hydroplaning Consideration. *Journal of Transportation Engineering*, **138**, 423-429. https://doi.org/10.1061/(ASCE)TE.1943-5436.0000336

[14] Guo, X.X., Zhang, C., Cui, B.X. and Wang, D. (2013) Analysis of Impact of Transverse Slope on Hydroplaning Risk Level. *Procedia-Social and Behavioral Sciences*, **96**, 2310-2319. https://doi.org/10.1016/j.sbspro.2013.08.260

[15] CAPVIDIA FlowVision HPC Version 3.09.05, 2016 User Manual.

[16] ABAQUS (2016) Analysis User's Manual, Version 6.16. Dassault Systemes Simulia, Inc., Johnston.

[17] Lindenmuth, B.E. (2006) An Overview of Tire Technology. National Highway Traffic Safety Administration, Washington DC, 2-27.

[18] Aksenov, A., Dyadkin, A. and Pokhilko, V. (1998) Overcoming of Barrier between CAD and CFD by Modified Finite Volume Method. *Proc.* 1998 *ASME Pressure Vessels and Piping Division Conference*, San Diego, ASME PVP-Vol. 377-1.

[19] Sung, M.F., Chen, C.F. and Chen, C.J. (2015) Using the CFD Technique to Analyze Tire Tread Hydroplaning Effects. *Asian Journal of Engineering and Technology*, **3**, 151-157